LUND UNIVERSITY

Effect of resonant impurity scattering on the carrier dynamics in Si/SiGe quantum wells

Vettchinkina, Valeria; Blom, Anders; Chao, Koung-An

Published in:
Physical Review B (Condensed Matter and Materials Physics)

DOI:
10.1103/PhysRevB.72.045303

2005

Link to publication

Citation for published version (APA):
Vettchinkina, V., Blom, A., & Chao, K.-A. (2005). Effect of resonant impurity scattering on the carrier dynamics in Si/SiGe quantum wells. *Physical Review B (Condensed Matter and Materials Physics)*, *72*(4). https://doi.org/10.1103/PhysRevB.72.045303

Total number of authors:
3

General rights
Unless other specific re-use rights are stated the following general rights apply:
Copyright and moral rights for the publications made accessible in the public portal are retained by the authors and/or other copyright owners and it is a condition of accessing publications that users recognise and abide by the legal requirements associated with these rights.
• Users may download and print one copy of any publication from the public portal for the purpose of private study or research.
• You may not further distribute the material or use it for any profit-making activity or commercial gain
• You may freely distribute the URL identifying the publication in the public portal

Read more about Creative commons licenses: https://creativecommons.org/licenses/

Take down policy
If you believe that this document breaches copyright please contact us providing details, and we will remove access to the work immediately and investigate your claim.

LUND UNIVERSITY

PO Box 117
221 00 Lund
+46 46-222 00 00

PHYSICAL REVIEW B **72**, 045303 (2005)

Effect of resonant impurity scattering on the carrier dynamics in Si/SiGe quantum wells

V. A. Vettchinkina, A. Blom, and K. A. Chao
Solid State Theory Division, Department of Physics, Lund University, Sölvegatan 14 A, S-233 62 Lund, Sweden
(Received 18 January 2005; revised manuscript received 3 May 2005; published 1 July 2005)

We have performed Monte Carlo simulations of the electron drift velocity in a δ-doped Si/SiGe quantum well, for high and low temperatures as well as strong and weak electric field. All scattering matrix elements of intervalley phonons, acoustic phonons, interface roughness, and impurity ions are calculated from the electron wave functions. Special attention was paid to the resonant state scattering which is far from understood both theoretically and experimentally. When the position of the δ-doped donor layer moves from the center of the quantum well to deep inside the barrier, we found for the first time the dramatic effect of the resonant state scattering on electron drift velocity. This effect is dominated by the resonant level broadening, which depends on the position of the δ-doped donor layer. Relative relaxation time of various scattering mechanisms was also derived from the Monte Carlo simulation.

DOI: 10.1103/PhysRevB.72.045303 PACS number(s): 73.63.Hs, 02.70.Uu, 72.20.Dp

I. INTRODUCTION

The physical properties of the two-dimensional (2D) electron gas are important not only for fundamental research but also for technological applications. Modern material fabrication techniques and advanced experimental facilities make it possible to measure these properties of high quality samples with high precision. Such valuable results provide a basis for 2D electronic devices.

Following the success of 2D electronic devices based on III-V semiconductor heterostructures, recently there has been much work done on strained Si or SiGe epilayers within silicon device technology. Taking advantage of the controllable lattice-mismatch induced strain, band-gap engineering allows the possibility to increase the carrier mobility in modulation doped heterostructures. One relevant key issue is to understand thoroughly the transport phenomena in the 2D electron gas confined in the Si layer and the various types of scattering event which take place in it. The measured carrier mobility, or drift velocity, contains the effects of all possible scattering mechanisms, and needs to be analyzed theoretically. For this purpose the Monte Carlo simulation is a very powerful approach. In Si/SiGe modulation doped structures the Monte Carlo simulation has given useful information on the electron transport properties.[1–4]

The purpose of conventional modulation doping is to increase the carrier mobility by separating the impurity ions from the transport channels. Under this situation, carriers are scattered mainly by phonons and interface roughness. However, a recent interesting topic is the resonant impurity scattering which plays an important role in the terahertz (THz) lasing from uniaxially strained bulk p-Ge.[5,6] The applied strain splits the heavy hole band and the light hole band. If the split is sufficiently large, the impurity levels attached to the upper hole band will be degenerate with the continuum of the lower hole band. A resonant state is then formed through hybridization of these two degenerate states, and the resulting energy level has a certain width. In the past the effect of impurity scattering on the carrier mobility of a semiconductor took into account only the conventional Coulomb scattering (CCS) channel by impurity ions. The presence of resonant states opens another impurity scattering channel which we call resonant state scattering (RSS) channel. How the RSS channel will affect the carrier mobility is an open question. To our knowledge, experiments on bulk doped semiconductors can hardly provide the answer.

Resonant states can also be formed in a doped quantum well in which the impurity levels attached to a higher subband will be degenerate with the 2D continuum of the lower subband. In connection to the possible THz radiation from Si/SiGe quantum wells, such resonant states were studied in detail very recently.[7] It was found that the width of the resonant level is very sensitive to the position of the impurity when the impurity is moved from the center of the well into the barrier. Therefore, in a δ-doped quantum well sample, the electron transport parallel to the interfaces will depend on the position of the δ-doping. This effect should also depend on the strength of an applied electric field which can inject hot carriers into the resonant states. In our opinion, the study of the hot carrier mobility or drift velocity in a δ-doped quantum well can give us valuable information on the characteristic features of resonant states.

The RSS channel has not been investigated before. In this paper we will perform a Monte Carlo simulation on the hot carrier drift velocity in a δ-doped Si/SiGe quantum well, taking into account all important scattering mechanisms including both the CCS channel and the RSS channel of the impurity scattering. The reliability of numerical results depends crucially on the accuracy of all the numbers appearing in the calculation. In our problem, to start with we must have the precise formula for all scattering probabilities. These formulas will be given in Sec. II, together with the electron eigensolutions based on which all scattering matrix elements are calculated. Section III gives a brief description on the specific procedure of Monte Carlo simulation of drift velocity. Focusing on the effect of resonant state scattering, the field and the temperature dependence of the calculated drift velocity in delta-doped Si/SiGe quantum wells are presented and discussed in Sec. IV. Within the scattering mechanism of impurity ions, the contributions of CCS channel and RSS channel are investigated in Sec. V. In the Monte Carlo simulation, we can keep track of the scattering mechanism of

 ©2005 The American Physical Society

each scattering. The relative relaxation times are then analyzed in Sec. VI. Our expectation on future parallel experimental investigation is expressed in Sec. VII.

II. SCATTERING PROBABILITY

Using the Monte Carlo approach to solve the Boltzmann transport equation we need to know the matrix elements of all relevant scattering processes. In a quantum well with growth direction along the z axis, the eigenstates

$$|\lambda\mathbf{k}\rangle = [e^{i\mathbf{k}\cdot\mathbf{r}}/L]\varphi_\lambda(z) \tag{1}$$

and the corresponding eigenenergies

$$E_{\lambda\mathbf{k}} = E_\lambda + E_\mathbf{k} \tag{2}$$

are specified by the subband index λ and the 2D wave vector $\mathbf{k}$. Here we assume a finite sample with a square cross section of area L^2 in the xy plane, and $\mathbf{r}=(r,\vartheta)$ is the position vector in cylindrical coordinates in this plane. In terms of the transverse effective mass $m_\parallel$, the 2D dispersion is simply

$$E_\mathbf{k} = \hbar^2 k^2/2m_\parallel. \tag{3}$$

The confined wave functions $\varphi_\lambda(z)$ satisfy the Schrödinger equation

$$\left(-\frac{\hbar^2}{2}\frac{\partial}{\partial z}\frac{1}{m_\perp(z)}\frac{\partial}{\partial z} + V(z)\right)\varphi_\lambda(z) = E_\lambda\varphi_\lambda(z), \tag{4}$$

where $m_\perp(z)$ is the spatially dependent longitudinal effective mass, and the potential $V(z)$ includes the effect of band bending if the doping concentration is large. We solve Eq. (4) self-consistently together with the Poisson equation.

Knowing these eigensolutions, we use the Fermi golden rule to calculate the transition rate

$$W(\lambda\mathbf{k};\lambda'\mathbf{k}') = \frac{2\pi}{\hbar}|M(\lambda\mathbf{k};\lambda'\mathbf{k}')|^2\delta(E_{\lambda'\mathbf{k}'} - E_{\lambda\mathbf{k}} - \Delta E) \tag{5}$$

from the initial state $|\lambda\mathbf{k}\rangle$ to the final state $|\lambda'\mathbf{k}'\rangle$, where ΔE is the energy change in an inelastic process. The scattering matrix element $M(\lambda\mathbf{k};\lambda'\mathbf{k}')$ depends on the individual scattering mechanism. For a given scattering mechanism, the total scattering rate $W(\lambda\mathbf{k})$ for scattering out of the state $|\lambda\mathbf{k}\rangle$ is the sum

$$W(\lambda\mathbf{k}) = \sum_{\lambda'\mathbf{k}'} W(\lambda\mathbf{k};\lambda'\mathbf{k}') \tag{6}$$

over all possible final states. If we define $\theta_{\mathbf{k}'}$ as the angle between $\mathbf{k}'$ and $\mathbf{k}$, then $W(\lambda\mathbf{k})$ is derived as

$$W(\lambda\mathbf{k}) = \frac{m_\parallel L^2}{2\pi\hbar^3}\sum_{\lambda'}\int_{E_{\lambda'}}^{\infty} dE'\int_0^{2\pi} d\theta_{\mathbf{k}'}|M(\lambda\mathbf{k};\lambda'\mathbf{k}')|^2\delta(E_{\lambda'\mathbf{k}'} - E_{\lambda\mathbf{k}} - \Delta E), \tag{7}$$

under the assumption of a parabolic dispersion as given in Eq. (3). The parabolic dispersion is valid near the bottom of each miniband. In typical realistic samples which will be investigated in this work, the separation between the two lowest subbands is about 35 meV, and the relevant resonant state energy is about 8 meV above the bottom of the lowest subband. Therefore, the use of a parabolic dispersion can provide a reliable description of resonant state scattering, which is the key issue of this paper. The nonparabolicity effect is important for hot electrons with energy far above the resonant state level. Consequently, it is reasonable to believe that this effect will not change the characteristic fetaures of the resonant state scattering qualitatively.

While focusing on the resonant state scattering by impurity ions, we should also mention the effect of electron-electron scattering. Since this scattering conserves the total momentum of the entire electron system, it has no effect on the electron mobility which will be studied in details in this paper. However, the electron-electron scattering contributes to the thermalization of the electron distribution. In order to demonstrate the effect of resonant state scattering with an analysis as unambiguous as possible, we have set such a low impurity concentration that the band bending is negligibly small. In this case, the thermalization process due to the electron-electron scattering is secondary to the primary process of electron-phonon scattering. In this respect, we have neglected the electron-electron scattering in our Monte Carlo simulation.

The energy relaxation in the conduction band of Si is produced by intervalley phonons, since the intravalley optical phonon scattering is forbidden by symmetry.[8,9] The intervalley scattering in Si consists of zero-order optical and first-order acoustic processes.[8,10] Besides these, the relevant elastic scattering mechanisms which randomize the momentum are produced by intravalley acoustic phonons, interface roughness, and impurities. The impurity scattering has two independent channels, ionized impurity scattering and resonant scattering. While the resonant scattering hardly has been studied before, all other scattering mechanisms have been much investigated in the past. Consequently, we will first present the final expressions of $W(\lambda\mathbf{k})$ for various *conventional* scattering mechanisms, and then discuss the resonant scattering in more details.

A. Conventional scattering

For the two intervalley phonon branches in our 2D system, the electron-phonon coupling $\mathcal{D}(\mathbf{q})$ has the simple form[8,10] $\mathcal{D}(\mathbf{q})=D_a|\mathbf{q}|$ for acoustic phonons with energy $\hbar\omega_a$, and $\mathcal{D}(\mathbf{q})=D_o$ for optical phonons with energy $\hbar\omega_o$. If we define

$$G_{\lambda\lambda'} = \int_{-\infty}^{\infty} |\varphi_\lambda(z)\varphi^*_{\lambda'}(z)|^2 dz, \tag{8}$$

$$H_{\lambda\lambda'} = \int_{-\infty}^{\infty} \varphi^*_\lambda(z)\varphi_{\lambda'}(z)\frac{d^2}{dz^2}[\varphi_\lambda(z)\varphi^*_{\lambda'}(z)]dz, \tag{9}$$

then the total scattering rate is[11]

$$W(\lambda\mathbf{k}) = \frac{D_a^2 m_\parallel}{2\hbar\rho\hbar\omega_a} N^{\pm}(\hbar\omega_a) \sum_{\lambda'} \Theta\left(\frac{\hbar^2 k^2}{2m_\parallel} \mp \hbar\omega_a + E_\lambda - E_{\lambda'}\right) \times \left[\left(2\frac{\hbar^2 k^2}{2m_\parallel} \mp \hbar\omega_a + E_\lambda - E_{\lambda'}\right)\frac{2m_\parallel}{\hbar^2} G_{\lambda\lambda'} - H_{\lambda\lambda'}\right] \tag{10}$$

for the first-order intervalley acoustic phonons, and

$$W(\lambda\mathbf{k}) = \frac{D_o^2 m_\parallel}{2\pi\hbar\rho\hbar\omega_o} N^{\pm}(\hbar\omega_o) \sum_{\lambda'} G_{\lambda\lambda'} \times \Theta\left(\frac{\hbar^2 k^2}{2m_\parallel} \mp \hbar\omega_o + E_\lambda - E_{\lambda'}\right) \tag{11}$$

for the zero-order intervalley optical phonons. In the above equations, ρ is the crystal mass density, and the step-function $\Theta(x)=1$ for positive x and $\Theta(x)=0$ for negative x. The quantity

$$N^{-}(\hbar\omega) \equiv N(\hbar\omega) = (e^{\hbar\omega/k_B T} - 1)^{-1} \tag{12}$$

is the phonon number, and $N^{+}(\hbar\omega)=N(\hbar\omega)+1$. $N^{+}(\hbar\omega)$ appears in a phonon emission process, and $N^{-}(\hbar\omega)$ in a phonon absorption process. We notice that except for the kinetic energy in the step function Θ, the zero-order intervalley optical scattering is actually independent of $\mathbf{k}$.

For temperatures above 77 K, the intravalley acoustic phonon scattering can be treated as an elastic process with the electron-phonon interaction[8] $\mathcal{D}(\mathbf{q})=D_{ac}|\mathbf{q}|$. At long wavelengths the phonon energy $\hbar\omega_{\mathbf{q}}$ is well approximated as $v_l|\mathbf{q}|$ where v_l is the longitudinal sound velocity. We then have

$$W(\lambda\mathbf{k}) = \frac{D_{ac} m_\parallel}{2\hbar^3 v_l^2 \rho} k_B T \sum_{\lambda'} G_{\lambda\lambda'} \Theta\left(\frac{\hbar^2 k^2}{2m_\parallel} + E_\lambda - E_{\lambda'}\right) \tag{13}$$

for intravalley acoustic phonon scattering. This scattering rate has a similar $\mathbf{k}$ dependence as that of intervalley optical phonons.

Since the interfaces are not perfectly flat, the spatial fluctuation $\delta L_w(\mathbf{r})$ of the well width L_w produces a spatial fluctuation

$$\delta E_\lambda(\mathbf{r}) = \frac{\partial E_\lambda}{\partial L_w} \delta L_w(\mathbf{r}) \tag{14}$$

of the subband energy E_λ. For a quantum well of finite depth, we may write[4]

$$\frac{\partial E_\lambda}{\partial L_w} = -\chi_\lambda \frac{\hbar^2 \lambda^2 \pi^2}{m_\parallel L_w^3}, \tag{15}$$

where χ_λ is a correction factor which is equal to unity for an infinitely deep well. χ_λ depends on the well depth, the subband index and the well width, and must be calculated numerically. The scattering due to such interface roughness is important at low temperatures,[12] and depends on the correlation function of $\delta L_w(\mathbf{r})$. Let Δ be the average amplitude of the well width fluctuation, and Λ the correlation length of the fluctuation. Assuming a Gaussian shape[13] for the correlation function

$$\langle \delta L_w(\mathbf{r}) \delta L_w(\mathbf{r}') \rangle = \Delta^2 e^{-|\mathbf{r}-\mathbf{r}'|^2/\Lambda^2}, \tag{16}$$

the total interface roughness scattering rate is derived as

$$W(\lambda\mathbf{k}) = \frac{\pi^4 \hbar \Delta^2 \Lambda^2 \chi_\lambda^2}{2 m_\parallel L_w^6} \int_0^{2\pi} d\theta e^{-\Lambda^2 k^2 (1-\cos\theta)/4}. \tag{17}$$

Finally we consider the scattering of carriers by a δ-doping layer of ionized donors located at z_0, with sheet concentration n_{2D}. The scattering by an ionized donor has two channels. The first channel which we call *conventional Coulomb scattering* (CCS) will be treated as conventional potential scattering, while the second *resonant state scattering* (RSS) channel will be analyzed in more details in the next section. As an approximation, which typically is well justified,[4,7] we can ignore the cross term (see below) and treat the two scattering channels independently.

The CCS process has been well documented in many quantum mechanics books. From these books, assuming a Thomas-Fermi screened dielectric constant ε_{TF}, we find the total scattering rate as[4]

$$W(\lambda\mathbf{k}) = \frac{e^2 m_\parallel}{4\pi^2 \hbar^3 \varepsilon_{TF}} n_{2D} \int_0^{2\pi} \left| \int_{-\infty}^{\infty} \frac{\exp[-|z-z_0| k\sqrt{2-2\cos\theta}]}{k\sqrt{2-2\cos\theta}} \times \phi_\lambda(z) \phi_{\lambda'}^*(z) dz \right|^2 d\theta. \tag{18}$$

B. Resonant scattering

Let us consider the scattering of an incoming carrier, with energy E and vector $\mathbf{k}$, by an impurity ion located at the origin. If there exists a localized state with energy close to E, it can capture the carrier and then re-emit it. Such a process through the formation of hybridized resonant states has been investigated recently both in p-doped bulk Ge (Ref. 14) and in 2D electron gases.[7,15] The complicated theory of resonant scattering in quantum wells can be much simplified if intersubband transitions are ignored. This will be the case to be studied in the present work.

Following the treatment of resonant scattering in three dimensions,[16] in our quantum well system the scattered wave function at large distances $\mathbf{r}=(r,\vartheta)$ from the scattering center can be written in the form

$$\psi_{\mathbf{k}}(\mathbf{r}) = e^{i\mathbf{k}\cdot\mathbf{r}} + \mu(\vartheta)\frac{e^{ikr}}{\sqrt{r}}. \tag{19}$$

By expanding the plane wave in its asymptotic form, and solving the free Schrödinger equation for large distances with proper boundary conditions, we can derive the scattering amplitude $\mu(\vartheta)$. For resonant scattering taking place at energy E^{res} with a width Γ, which is related to the lifetime τ of the resonant state as $\Gamma=\hbar/\tau$, we obtain

$$\mu(\vartheta) = -\alpha - \frac{1}{\sqrt{2\pi k}}\frac{\Gamma}{E - E^{\rm res} + i\Gamma/2}\sum_m e^{-im\vartheta}e^{2i\delta_m^{(0)}}. \quad (20)$$

Here α represents the CCS channel, and the rest of $\mu(\vartheta)$ is for the RSS channel. Γ is typically of the order 1 meV, and therefore the RSS scattering probability has a sharp and localized peak. On the other hand, the CCS scattering probability, Eq. (18), is a smooth function of the electron energy with a dominant contribution around $k=0$. Consequently, the cross term between the CCS and the RSS channel can be ignored, as mentioned at the end of the preceding section. Moreover, the phase shifts $\delta_m^{(0)}$ in the second term on the right-hand side of Eq. (20) can be approximated by unity.[16]

We will then ignore the α in $\mu(\vartheta)$ to investigate the RSS channel. In our problem it is sufficient to retain only the s-wave scattering with the $m=0$ term in the sum in Eq. (20). We can then write the RSS amplitude for the initial state $|\lambda\mathbf{k}\rangle$ as

$$\mu_{\lambda\mathbf{k}}(\vartheta) = -\frac{1}{\sqrt{2\pi k}}\frac{\Gamma_\lambda}{E_{\lambda\mathbf{k}} - E_\lambda^{\rm res} + i\Gamma_\lambda/2}. \quad (21)$$

In the above expression, we have neglected the weak $\mathbf{k}$ dependence of Γ_λ and $E_\lambda^{\rm res}$. The exact values of these quantities can be evaluated using the resonant coupling approach.[15] The resonant scattering cross section, which has the dimension of length for a 2D system, is defined as

$$\sigma_{\lambda\mathbf{k}} = \int_0^{2\pi}|\mu_{\lambda\mathbf{k}}(\vartheta)|^2 d\vartheta = \frac{\Gamma_\lambda^2/k}{(E_{\lambda\mathbf{k}} - E_\lambda^{\rm res})^2 + \Gamma_\lambda^2/4}. \quad (22)$$

In terms of $\sigma_{\lambda\mathbf{k}}$ and the particle velocity $\hbar k/m_\parallel$ the total rate of resonant scattering has the simple form

$$W(\lambda\mathbf{k}) = n_{\rm 2D}\frac{\hbar k}{m_\parallel}\sigma_{\lambda\mathbf{k}}. \quad (23)$$

III. MONTE CARLO SIMULATION

The two commonly used approaches for Monte Carlo simulations in semiconductors are single-particle and ensemble simulations. If the system to be investigated exhibits strong carrier-carrier correlation, or involves a time-dependent response to an external stimulation, it is necessary to use the ensemble Monte Carlo approach. However, we will study the transport properties of independent carriers in semiconductors under an applied homogeneous electric field. Although several different scattering mechanisms are taken into account, we do not include carrier-carrier correlation nor impact ionization. Hence, it is proper to use the standard single-particle Monte Carlo technique which was developed for carrier transport in semiconductors.[17]

There are two methods to calculate the drift velocity of the carriers. One can first simulate the carrier distribution function in momentum space, and then average the momentum with this distribution to obtain the velocity. One can also simulate the drift velocity directly without using the distribution function; that is the approach we have adopted, and thus we simulate the distribution function and the drift velocity simultaneously. In this way it is possible to use the distribution function to check the convergence of the simulation. Furthermore, without any applied electric field the distribution function is spherically symmetric due to thermalization, but will become asymmetric when the field is turned on. Such information of the distribution function *stretching* along the field direction will be very useful for the understanding of the calculated drift velocity.

Because the dynamical processes in our Monte Carlo simulation include intervalley scattering, it is necessary to specify the electron eigenstate $|\lambda\mathbf{k}j\rangle$ in a Si/SiGe quantum well by the subband index λ, the 2D wave vector $\mathbf{k}$, and the valley index j. Because the bulk symmetry is broken in layer structures, in a Si/SiGe quantum well there are only two low-lying valleys to take into account.[18] Under an applied dc electric field $\mathcal{E}$ parallel to interfaces, an electron will perform *free-flight* motion between two collisions. During the free-flight motion only the wave vector $\mathbf{k}$ changes with time; specifically, it evolves linearly as the carrier is accelerated by the field. Conversely, when an electron is scattered by one of the various scattering mechanisms, its state changes instantaneously from $|\lambda\mathbf{k}j\rangle$ to $|\lambda'\mathbf{k}'j'\rangle$. We will label the free-flight time intervals by l, and specify the lth time interval as from $t_{l,i}$ to $t_{l,f}$. Let $\mathbf{V}[\mathbf{k}(t)]$ be the velocity during the free flight. Then the drift velocity $\mathbf{V}_{dr}(\mathcal{E})$ is calculated as[17]

$$\mathbf{V}_{dr}(\mathcal{E}) = \frac{1}{T}\sum_l \int_{t_{l,i}}^{t_{l,f}} \mathbf{V}[\mathbf{k}(t)]dt, \quad (24)$$

where $T=\Sigma_l(t_{l,f}-t_{l,i})$ is the total duration of the Monte Carlo simulation.

To perform the Monte Carlo simulation, we keep track of the momentum changes during each free flight, and then take a proper average. In practice it is more convenient to average over the energy. We will simplify the notation by defining $\mathbf{k}_{l,i}=\mathbf{k}(t_{l,i})$ and $\mathbf{k}_{l,f}=\mathbf{k}(t_{l,f})$ as the initial and final wave vectors of the free-flight interval l, and we also introduce $K=e\mathcal{E}T/\hbar$. Using the relation

$$\mathbf{V}_{\lambda,j}(\mathbf{k}) = \frac{1}{\hbar}\nabla_\mathbf{k}E_{\lambda,j}(\mathbf{k}), \quad (25)$$

where $E_{\lambda,j}(\mathbf{k})$ is the 2D subband energy with explicit reference to the jth valley, we can rewrite Eq. (24) as

$$\mathbf{V}_{dr}(\mathcal{E}) = \frac{1}{K}\sum_l \int_{\mathbf{k}_{l,i}}^{\mathbf{k}_{l,f}} \frac{1}{\hbar}\nabla_\mathbf{k}E_{\lambda(l),j(l)}(\mathbf{k})d\mathbf{k} = \frac{1}{\hbar K}\sum_l [E_{\lambda(l),j(l)}(\mathbf{k}_{l,f}) - E_{\lambda(l),j(l)}(\mathbf{k}_{l,i})], \quad (26)$$

where we have explicitly indicated that both the subband and valley index are functions of the interval label l. When using this equation to simulate the drift velocity for different temperatures under various applied electric fields, the convergence of the Monte Carlo results presented below has been checked carefully.

To produce the Monte Carlo numerical results, we first derive the eigensolutions from the Schrödinger equation (4) in a $\mathrm{Si/Si}_x\mathrm{Ge}_{1-x}$ quantum well using well-known values of the electron effective mass, band offsets, and deformation potentials.[18] The details of the calculation can be found in

Ref. 7. With these eigensolutions one can calculate all the relevant scattering rates given in the preceding section, and the Monte Carlo calculation can then be performed. The obtained results will be presented in the following two sections.

IV. DRIFT VELOCITY

The system we have investigated is a $Si/Si_{0.80}Ge_{0.20}$ quantum well with the width 50 Å. The system contains a δ-doping layer at the position z_0 which varies from the center of the well $z=0$ to deep inside the barrier. Because the system is symmetric, we will only consider $z_0>0$. We have chosen a relatively low donor concentration $n_{2D}=5\times10^{10}$ cm^{-2}. In this case the band-bending effect is negligibly small, and although the Pauli exclusion principle is included in the Monte Carlo simulation, the calculated results indicate that it does not play an important role. For this configuration the lowest antisymmetric impurity state which is attached to the bottom of the second quantum well subband becomes resonant with the continuum of the first subband.

Since the carriers are confined mainly in the quantum well, the phonon scattering is insensitive to the position of the δ-doping layer. As the impurity ions are moved into the barrier region, the weakening Coulomb force on the carriers should result in a monotonically increasing carrier drift velocity. This expectation is correct if only the CCS channel contributes, but it is no longer so when the RSS channel is included because the width of the resonant level $\Gamma(z_0)$ depends on the position z_0 in a complicated way.[7] In fact, in the present sample structure, $\Gamma(z_0)$ attains its maximum value when z_0 is in the quantum well and about 8 Å from one interface. Such behavior of the broadening of the resonant level also introduces a weak dependence of the interface roughness scattering on the position of the δ-doping layer. Consequently, we are mostly interested in the effect of resonant scattering on the carrier drift velocity.

The important physics of the carrier drift velocity is its dependence on the temperature T and the applied electric field $\mathcal{E}$. For semiconducting systems, the most relevant temperature range is from liquid nitrogen temperature to room temperature, and the most commonly applied electric field strength is up to a few kV/cm. Hence, we will analyze our numerical results for two temperatures 100 K and 300 K, and two electric field strengths 300 V/cm and 3000 V/cm. For each of the four cases we will present the carrier drift velocity calculated with and without the resonant scattering mechanism included.

Under an external electric field strength 300 V/cm, the Monte Carlo simulated carrier drift velocity is shown in Fig. 1 vs the δ-doping layer position z_0. Let us first analyze the open circles which are calculated drift velocity without the resonant scattering. As the impurity ions move away from the well center $z_0=0$ into the barrier, the drift velocity remains almost constant until the impurities are near to one interface marked by the vertical dotted line. Then the drift velocity increases rapidly when the impurities move deep into the barrier region. This is a clear illustration of the principle of modulation doping for achieving high carrier mobility.

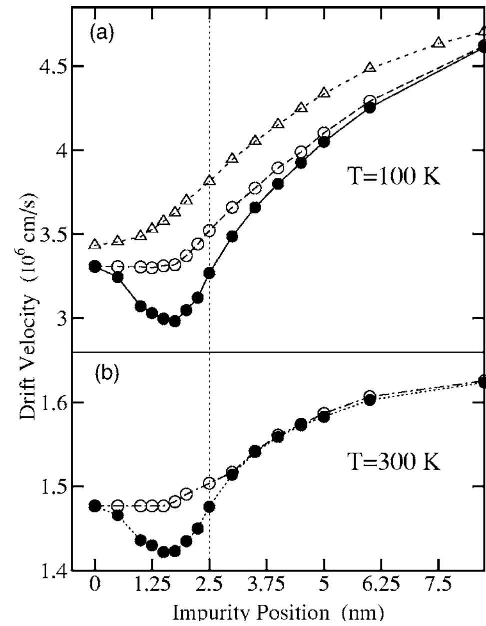

FIG. 1. The Monte Carlo simulated drift velocity for an applied electric field 300 V/cm, at the temperature 100K [panel (a)] and 300 K [panel (b)]. The center of the quantum well is at position 0, and the dotted vertical line marks the well interface. In each panel, the open (solid) circles are the drift velocity calculated excluding (including) the resonant scattering. The triangles in the upper panel refer to a simulation where both interface roughness scattering and resonant scattering were excluded. Note that the vertical scales are different in the two panels.

When we include the resonant scattering in our Monte Carlo simulation, the drift velocity is suppressed, as indicated by the solid circles in Fig. 1. We notice the appearance of a minimum in the drift velocity around the impurity position $z_0\simeq17.5$ Å (i.e., about 7.5 Å from the interface). The difference between the open circles and the solid circles is the drift velocity change due to the resonant scattering. Starting from zero at z_0, this difference grows to a maximum and then reduces to zero as z_0 increases. The level position and the width $\Gamma(z_0)$ of the resonant state as functions of z_0 were studied in details in Ref. 7. At the center of the well, symmetry implies that $\Gamma(z_0=0)=0$. The width increases as z_0 approaches one interface, reaching its maximum value before the impurity ion moves across the interface into the barrier. Moving away from the interface deep into the barrier, $\Gamma(z_0)$ diminishes to zero. Consequently, the effect of resonant scattering on the drift velocity is determined by the level broadening $\Gamma(z_0)$.

The degree of influence of resonant scattering is also closely related to the binding energy of the resonant impurity state. The resonance energy level in our system lies just above the bottom of the lowest subband,[7] with about 8.4 meV separation at $z_0\simeq17.5$ Å. At this position of z_0, the broadening $\Gamma(z_0)$ reaches its maximal value 7.5 meV. The calculated distribution function reveals that there is a significant increase of carriers in the region around the resonance. We will return to illustrate this phenomenon at the end of this section.

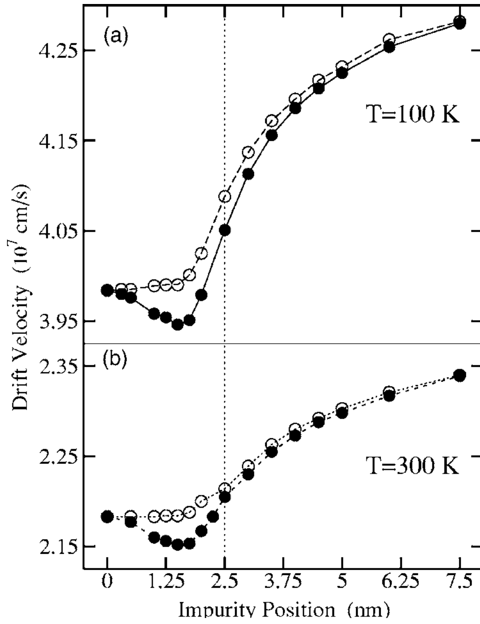

FIG. 2. The Monte Carlo simulated drift velocity for an applied electric field 3000 V/cm, at the temperature 100 K [panel (a)] and 300 K [panel (b)]. Symbols as in Fig. 1.

One would expect that the effect of interface roughness scattering on the carrier drift velocity will not be coupled to the position of the δ-doping layer, since the carriers are confined to the quantum well by the two interfaces. This is however not so in the presence of resonant states, which are hybridized states of the continuous subband states and the localized impurity orbitals. Because of this modification of the spatial probability distribution of carriers around the impurities, the effect of interface roughness scattering has a weak dependence on the impurity position. To illustrate this aspect, we repeat the drift mobility calculation excluding both resonant scattering and interface roughness scattering. The so-obtained result for $T=100$ K and $\mathcal{E}=300$ V/cm is plotted in panel (a) of Fig. 1 as open triangles. We see that as the impurities are moved from the center of the quantum well to a location deep inside the barrier, the difference between the open triangles and the open circles, which represents the effect of interface roughness scattering, is correlated to the broadening $\Gamma(z_0)$ of the resonant states.

Figure 2 shows the calculated carrier drift velocity under the acceleration of a higher electric field $\mathcal{E}=3000$ V/cm, at two temperatures $T=100$ K and $T=300$ K. As expected, here the drift velocity is one order of magnitude higher than that for the low field situation in Fig. 1. Again, the difference between the open circles and the solid circles follows the characteristic feature of the broadening $\Gamma(z_0)$ of the resonant states.

All scattering processes can be traced out step by step during our Monte Carlo simulation. This enables us to understand the temperature and field dependence of the results shown in Figs. 1 and 2. Acoustic phonon scattering is the major mechanism that limits the carrier drift velocity, and the interface roughness scattering is always present under any condition. While both intervalley optical and acoustic phonon scattering provide important energy relaxation channels if the applied field is strong, in the low field situation only elastic acoustic phonon scattering randomizes the momenta in the distribution function. However, a strong electric field can stretch the distribution function and so modifies it significantly. In the absence of resonant state scattering, all these phenomena were analyzed in details in Ref. 4. Here we will analyze the influence of resonant state scattering on the distribution function.

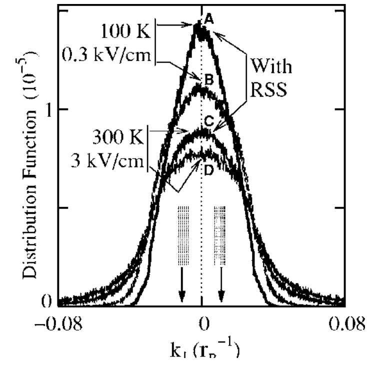

FIG. 3. Electron momentum distribution along the momentum component $k_\perp$ perpendicular to the field direction, for a δ-doping layer at $z_0=17.5$ Å. The resonant energy level and the corresponding $\Gamma(z_0)$ are marked by arrows and the shadded regions, respectively.

For the two-dimensional momentum **k** parallel to the interfaces, let $k_\parallel$ be the component parallel to the applied electric field, and $k_\perp$ the perpendicular component. At $z_0=17.5$ Å where $\Gamma(z_0)$ has its maximal value, the corresponding distribution function along $k_\perp$ is shown in Fig. 3 for both the low field low temperature case ($\mathcal{E}=300$ V/cm, $T=300$ K) and the high field high temperature case ($\mathcal{E}=300$ V/cm, $T=300$ K). The units for the momentum is inverse Bohr radius r_B^{-1}. Because the momentum component is perpendicular to the field direction, all curves are symmetric. Curves B and D are derived without the resonant state scattering, and they are simular to those presented in Ref. 4. We should mention that curve B broadens to curve D with increasing temperature and/or field strength.

In momentum space, the corresponding position of the resonant energy level is marked by the two downwards heavy arrows, and around each arrow the region corresponding to the broadening width $\Gamma(z_0)$ is indicated by the shadded area. Curves A and C are calculated with the resonant state scattering included. It is clearly seen that the resonant state scattering enhances the distribution function in the energy regime around the resonant energy level. This enhancement decreases with increasing temperature and/or field strength.

The distribution function along the component $k_\parallel$ parallel to the field is given in Fig. 4. We see the similar type of enhancement exhibited in Fig. 3. However, because of the field stretching, all curves are highly asymmetric and shifted along the field direction.

V. EQUIVALENT IMPURITY CONCENTRATION

As discussed above, we have treated the two impurity scattering channels, CCS and RSS, as mutually exclusive.

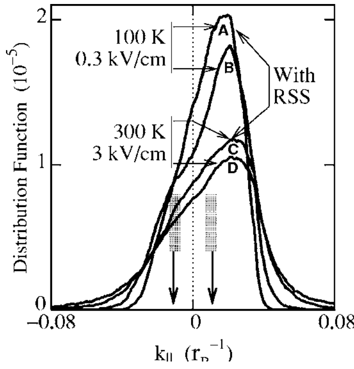

FIG. 4. Distribution function for momentum component $k_{\|}$ parallel to the field direction, for a δ-doping layer at $z_0=17.5$ Å. The resonant energy level and the corresponding $\Gamma(z_0)$ are marked by arrows and the shadded regions, respectively.

One way to estimate the relative efficiency of these two channels is to find out how many additional impurity ions that are required to maintain the same value of the drift velocity if the resonant scattering channel is blocked.

Earlier we set the impurity concentration to $n_{2D}=5\times10^{10}$ cm^{-2} in our Monte Carlo simulation. We will now attempt to increase the impurity concentration, in order to produce the same drift velocity from a Monte Carlo simulation where resonant scattering is excluded. The required concentration n^*_{2D} will depend on the applied electric field, the temperature, the position z_0 of the δ-doping layer, as well as the original density n_{2D}. We define the difference $\Delta n_{2D}(\mathcal{E},T,z_0)=n^*_{2D}-n_{2D}$ as the *equivalent impurity concentration*, meaning that it is an artificial additional doping concentration which simulates the effect of the RSS channel.

The calculated normalized equivalent impurity concentration $\Delta n_{2D}(\mathcal{E},T,z_0)/n_{2D}$ for $T=100$ K and $z_0=17.5$ Å is plotted in Fig. 5 as a function of the applied field. The ratio $\Delta n_{2D}/n_{2D}$ decreases monotonically from 0.42 for low fields to 0.2 for high fields. This behavior is due to the field stretching of the distribution function. As we mentioned earlier, under low field and at low temperature, the carrier momentum is randomized by elastic acoustic phonon scattering. This process produces a significant amount of carriers in the energy region around the resonance energy level, and so assists in producing efficient resonant scattering. When the electric field strength is increased, the distribution function is stretched along the field direction due to the carrier streaming motion. The amount of carriers around the resonance energy level is then reduced and so the ratio $\Delta n_{2D}/n_{2D}$ decreases monotonically. Thermal excitation of carriers can also decrease the value of the equivalent impurity concentration, especially for the situation of low electric field. To demonstrate this feature, we have performed a similar Monte Carlo simulation for a higher temperature $T=300$ K. We found that the ratio decreases from $\Delta n_{2D}/n_{2D}=0.34$ at $\mathcal{E}=300$ V/cm to $\Delta n_{2D}/n_{2D}=0.2$ at $\mathcal{E}=3000$ V/cm.

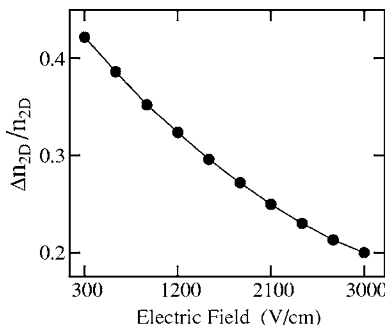

FIG. 5. Normalized equivalent impurity concentration $\Delta n_{2D}/n_{2D}$ with a δ-doping layer at $z_0=17.5$ Å.

TABLE I. Relative relaxation times for the mechanisms which are insensitive to the δ-doping layer position.

[$\mathcal{E}$ (V/cm); T (K)]	τ_{ivac}/τ_{ac}	τ_{ivop}/τ_{ac}	τ_{infs}/τ_{ac}
[300; 100]	29.47	48.73	4.30
[300; 300]	27.44	18.11	14.38
[3000; 100]	3.87	1.82	14.55
[3000; 300]	13.64	6.78	25.70

VI. RELATIVE RELAXATION TIME

In this section we will demonstrate how it is possible to extract information about the relaxation times associated with each scattering mechanism from the Monte Carlo simulation.

In a Monte Carlo simulation for given values of the electric field $\mathcal{E}$, the temperature T, and the position of the δ-doping layer z_0, we follow the motion of the carriers undergoing various types of scattering. In each scattering event, we record by which mechanism the carrier is scattered. After the simulation has converged and we have obtained the steady-state distribution function, we may continue to run the Monte Carlo process for a large number, $\mathcal{N}$, of scattering events, and during the simulation we record the total number of times $\mathcal{N}_i$ the carrier is scattered by each respective mechanism i. For a large value of $\mathcal{N}$ (of the order 10^7), the ratio

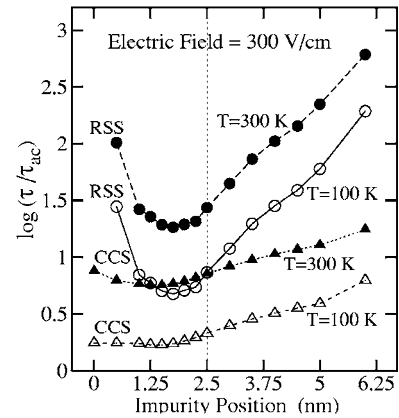

FIG. 6. Relative relaxation times for an applied field 300 V/cm at temperatures 100 K (open symbols) and 300 K (solid symbols). The curves marked CCS are for conventional Coulomb scattering, and RSS for resonant scattering. The vertical dotted line marks one interface.

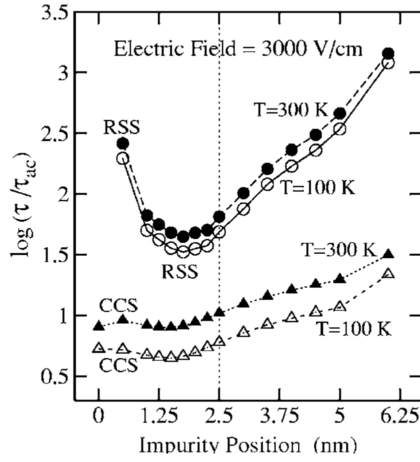

FIG. 7. Relative relaxation times for an applied field 3000 V/cm at temperatures 100 K (open symbols) and 300 K (solid symbols). The curves marked CCS are for conventional Coulomb scattering, and RSS for resonant scattering. The vertical dotted line marks one interface.

$\mathcal{N}_i/\mathcal{N}$ always converges to a constant value for all scattering mechanisms.

Let τ_i be the relaxation time for the ith scattering mechanism, corresponding to $\mathcal{N}_i$ scattering events. We can normalize the relaxation time τ_i with respect to the relaxation time τ_{ac} for intravalley acoustic phonons, which is the most well-studied relaxation time both theoretically and experimentally, and is known for many cases. Using the relation

$$\frac{\tau_i}{\tau_{ac}} = \frac{\mathcal{N}_{ac}}{\mathcal{N}_i}, \tag{27}$$

the *relative relaxation times* for all scattering mechanisms can be calculated.

For given field strength and temperature, the relative relaxation times τ_{ivac}/τ_{ac} for intervalley acoustic phonons, τ_{ivop}/τ_{ac} for intervalley optical phonons, and τ_{infs}/τ_{ac} for interface roughness are highly insensitive to the position of the δ-doping layer, as expected. These values are given in Table I.

On the other hand, the relative relaxation times $\tau_{\text{ccs}}/\tau_{ac}$ for the CCS channel and $\tau_{\text{rss}}/\tau_{ac}$ for the RSS channel of the impurity scattering are very sensitive to the impurity position z_0. The Monte Carlo simulated results are shown in Fig. 6 for the lower electric field 300 V/cm, and in Fig. 7 for the higher electric field 3000 V/cm. When the δ-doping layer moves from inside the quantum well deep into the barrier, $\tau_{\text{ccs}}/\tau_{ac}$ increases slowly. However, for the resonant scattering, we observe a smaller value of $\tau_{\text{rss}}/\tau_{ac}$ for a larger value of the broadening $\Gamma(z_0)$ of the resonant energy level. At the center of the quantum well $\Gamma(z_0)=0$ because of symmetry. Consequently, at $z_0=0$ the value of $\tau_{\text{rss}}/\tau_{ac}$ becomes infinite, which is consistent with the effect of resonant scattering on the drift velocity shown in Figs. 1 and 2.

It is important to note that in logarithmic scale all $\tau_{\text{rss}}/\tau_{ac}$ curves in Figs. 6 and 7 have almost the same shape. The effect of the applied field strength and the temperature is just to move the curves up or down almost rigidly. Because of its negligible dependence on the impurity position z_0, the relaxation time for acoustic scattering can be specified explicitly as $\tau_{ac}(\mathcal{E},T)$. Then, the *rigid-shift* phenomenon suggests an explicit form $\tau_{\text{rss}}(\mathcal{E},T,z_0) \simeq \xi_1(\mathcal{E},T)\xi_2(z_0)$ for the resonant scattering relaxation time. Consequently, we have $\log(\tau_{\text{rss}}/\tau_{ac}) = \log[\xi_1(\mathcal{E},T)/\tau_{ac}(\mathcal{E},T)] + \log[\xi_2(z_0)]$. The z_0-dependent curve $\log[\xi_2(z_0)]$ is shifted rigidly by the factor $\log[\xi_1(\mathcal{E},T)/\tau_{ac}(\mathcal{E},T)]$ as the field $\mathcal{E}$ or the temperature T changes. This interpretation finds its support in Eq. (22) for the resonant scattering cross section $\sigma_{\lambda\mathbf{k}}$. To calculate the relaxation time $\tau_{\text{rss}}(\mathcal{E},T,z_0)$, we need to multiply $\sigma_{\lambda\mathbf{k}}$ with the distribution function and integrate over the energy $E_{\lambda\mathbf{k}}$. Since the distribution function is very smooth within the small energy interval Γ_λ, the Γ_λ in the denominator of Eq. (22) can be neglected when performing the integration. In this way the integration over $E_{\lambda\mathbf{k}}$ yields the function $\xi_1(\mathcal{E},T)$, and $\xi_2(z_0)$ is actually a function of the level broadening Γ_λ. This argument explains well the behavior of $\tau_{\text{rss}}/\tau_{ac}$ in Figs. 6 and 7.

In Figs. 6 and 7 all $\tau_{\text{ccs}}/\tau_{ac}$ curves also have the same shape. To explain this phenomenon following the above argument, one should start from Eq. (18). The algebraic work is however much more complicated and requires lengthy calculations.

VII. CONCLUSIONS

Only recently has the physics of resonant states in doped semiconductors and their heterostructures emerged as an important research topic, and until now the effect of these states on the carrier mobility has been completely unknown. To clarify this issue we have performed a Monte Carlo simulation, which takes into account all relevant scattering mechanisms in their proper form for a 2D electron gas, to reveal the profound influence of resonant scattering on the carrier dynamics in Si/SiGe quantum wells containing a δ-doping layer of shallow impurities. Hopefully the present work will stimulate more studies on the dynamical aspects of resonant scattering both theoretically and experimentally.

ACKNOWLEDGMENTS

This work was supported by the Swedish Research Council (Grant No. 621-2002-3774), and the Swedish Foundation for International Cooperation in Research and Higher Education.

[1] H. Miyata, T. Yamada, and D. K. Ferry, Appl. Phys. Lett. **62**, 2661 (1993).
[2] T. Yamada, J.-R. Zhou, H. Miyata, and D. K. Ferry, IEEE Trans. Electron Devices **41**, 1513 (1994).
[3] P. Dollfus, J. Appl. Phys. **82**, 3911 (1997).
[4] V. A. Vettchinkina, A. Blom, and M. A. Odnoblyudov, Int. J. Mod. Phys. B (to be published).
[5] I. V. Altukhov, E. G. Chirikova, M. S. Kagan, K. A. Korolev, V. P. Sinis, and F. A. Smirnov, Sov. Phys. JETP **74**, 404 (1992).
[6] M. A. Odnoblyudov, I. N. Yassievich, M. S. Kagan, Yu. M. Galperin, and K. A. Chao, Phys. Rev. Lett. **83**, 644 (1999).
[7] A. Blom, M. A. Odnoblyudov, I. N. Yassievich, and K. A. Chao, Phys. Rev. B **68**, 165338 (2003).
[8] B. K. Ridley, *Quantum Processes in Semiconductors*, 2nd ed. (Clarendon, Oxford, 1988).
[9] P. Y. Yu and M. Cardona, *Fundamentals of Semiconductors*, 2nd ed. (Springer-Verlag, Berlin, 1999).
[10] D. K. Ferry, Phys. Rev. B **14**, 1605 (1976).
[11] F. Monsef, P. Dollfus, S. Galdin, and A. Bournel, Phys. Rev. B **65**, 212304 (2002); **67**, 059903(E) (2003).
[12] B. Laikhtman and R. A. Kiehl, Phys. Rev. B **47**, 10515 (1993).
[13] H. Sakaki, T. Noda, K. Hirakawa, M. Tanaka, and T. Matsusue, Appl. Phys. Lett. **51**, 1934 (1987).
[14] M. A. Odnoblyudov, I. N. Yassievich, V. M. Chistyakov, and K. A. Chao, Phys. Rev. B **62**, 2486 (2000).
[15] A. Blom, M. A. Odnoblyudov, I. N. Yassievich, and K. A. Chao, Phys. Rev. B **65**, 155302 (2002).
[16] L. D. Landau and E. M. Lifshitz, *Quantum Mechanics. Non-Relativistic Theory*, 3rd ed. (Pergamon, Oxford, 1977).
[17] C. Jacoboni and L. Reggiani, Rev. Mod. Phys. **55**, 645 (1983).
[18] M. M. Rieger and P. Vogl, Phys. Rev. B **48**, 14576 (1993).